Pattern Formation in a Twisted Nematic Liquid Crystal Cell under an External Magnetic Field

Luca Carlotti, Sandro Faetti, Maurizio Nobili

J. Phys. II France 6 (1996) 235–253 FEBRUARY 1996, PAGE 235

Pattern Formation in a Twisted Nematic Liquid Crystal Cell under an External Magnetic Field

Luca Carlotti, Sandro Faetti(*) and Maurizio Nobili

INFM and Dipartimento di Fisica dell'Università di Pisa, Piazza Torricelli 2, 56126 Pisa, Italy

(Received 22 May 1995, revised 18 September 1995, accepted 6 November 1995)

PACS.61.30.-v – Liquid crystals

Abstract. — We analyze the spatially inhomogeneous dynamic behaviour of a $+\pi/2$ twisted NLC layer in a magnetic field. When a magnetic field H is applied in the layer plane at a suitable angle β with respect to the easy axis on the first surface, the relaxation toward the equilibrium texture occurs through a slow decay of unstable textures. For some values of β and H, the relaxation of the unstable texture is strongly inhomogeneous and spatial domains occur everywhere. In this special case, a very rich dynamical behaviour is observed together with the appearance of domains corresponding to unstable, metastable, and stable textures coupled with line defects and walls. We have studied and modelled the form and the properties of the different domains and interfaces, the velocities of the defect lines and the inhomogeneous-homogeneous character of the unstable texture relaxation. The static and dynamic features of the observed domains are in satisfactory agreement with the theoretical predictions.

1. Introduction

The relaxation of nematic nematic liquid crystals (NLC) subjected to external orientation fields has been extensively investigated in the literature (see, for instance [1] and references therein). Because of the non-linear nature of these media, the relaxation toward the equilibrium state occurs often through the appearance of dynamical transitory textures [2, 3]. The study of these transient phenomena is very important in order to reach a better comprehension of the dynamic properties of non-linear systems. So far, most experiments have been made using uniformly aligned NLC layers subjected to magnetic or electric fields.

In this paper, we study the transient textures that appear when a twisted NLC layer is subjected to a magnetic field parallel to the layer. A lot of transitory textures are observed when the magnetic field is switched on, depending on the intensity and the orientation of the magnetic field. All these textures are interpreted using the Leslie-Enricksen hydrodynamic theory of NLCs.

The NLC sample is sandwiched between two parallel glass plates that are treated to induce a homogeneous surface alignment along two orthogonal axes in the plane of the plates. The initial alignment in the NLC layer is a uniform $+\pi/2$ twist along the $z-$axis orthogonal to the plates, and a magnetic field $\mathbf{H}$ is applied in the $x-y$ plane. The angle β, between the magnetic field $\mathbf{H}$ and the easy axis on the lower glass plate, plays a very important role. For

(*) Author for correspondence (e-mail: faetti@ipifidpt.difi.unipi.it)

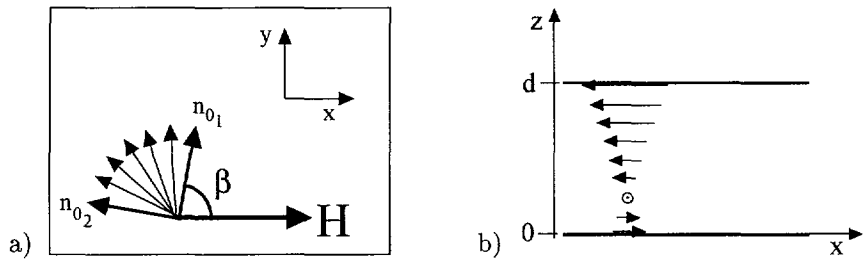

Fig. 1. — Director orientation in the pre-twisted NLC layer. $\mathbf{n}_{0_1}$ and $\mathbf{n}_{0_2}$ are the easy axes on the two plane surfaces. The magnetic field **H** is applied parallel to the $x-$axis. **z** is the normal to the two plane surfaces positioned in $z = 0$ and $z = d$. (a) Top view. (b) Side view.

$0 < \beta < \pi/2$, the relaxation toward the equilibrium is characterized by the occurrence of slow decay unstable textures. The relaxation time τ_W depends exponentially on the $\beta-$angle and can be much longer than τ_R, the typical relaxation time of a uniformly aligned NLC cell. This special feature makes the dynamic response extremely sensitive to the uniformity of the surface alignment. In particular, small inhomogeneities of the surface director alignment make τ_W a function of the $x - y$ coordinates. Depending on the intensity of the magnetic field and on the β-angle, we observe two very different regimes: a nearly homogeneous regime and a strongly inhomogeneous regime. In the first case, only small spatial dishomogeneities can be observed on the NLC layer. This dynamical regime has been extensively investigated in [4]. In the second case, the relaxation toward the stationary state occurs through nucleation of domains corresponding to unstable, metastable and stable textures. We have studied the form and the properties of the different domains and interfaces, the velocities of the defect lines [5, 6] and the character of the unstable-to-metastable texture transition.

The plan of the paper is as follows: in Section 2.1 we describe the experimental apparatus and method. The observed dynamical domains are shown in Section 2.2. In Section 3, we characterize the observed domains with the corresponding stationary (3.1 and 3.2) and transient textures (3.3). The form and structure of the different domains and interfaces are studied in Section 4. The dynamic behaviour is analyzed in Section 5, where line speeds are measured in Section 5.1 and a simple model to explain the inhomogeneous relaxation of the unstable texture is given in Section 5.2. Finally, in Section 6 we draw our conclusions.

2. Experiment

2.1. Experimental Apparatus and Method. — The experimental apparatus consists of a planar cell filled with 4−pentyl 4′−cyanobiphenyl (5CB) and placed in between the two poles of a Brucker electromagnet, giving a magnetic field up to 7.7 kG. The NLC is regulated at $T = 25 \pm 0.01$ °C. The two glass plates forming the cell are treated by SiO evaporation. The SiO thickness s_{SiO} and the SiO evaporation angle α_{SiO} are $s_{SiO} = 450$ Å and $\alpha_{SiO} = 60°$, well inside the planar anchoring region of the $\alpha_{SiO} - s_{SiO}$ phase diagram [7]. The two glass plates are mounted with the easy axes perpendicular to each other so that a uniform $\pi/2$ twist distortion is present in the cell (see Fig. 1). A magnetic field **H** can be applied along the **x** axis in the plane of the NLC layer ($x - y$ plane). β and $\beta + \pi/2$ represent the angles of the two easy axes at the surfaces $z = 0$ and $z = d$, with respect to the magnetic field (d is the cell thickness).

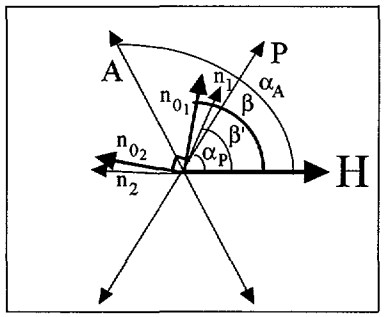

Fig. 2. — The polarizer P and the analyzer A make the angles α_P and α_A as regards to the magnetic field $\mathbf{H}$, respectively. The solid vectors $\mathbf{n}_{0_1}$ and $\mathbf{n}_{0_2}$ represent the easy directions at the first and at the second interface, respectively. β is the angle between $\mathbf{n}_{0_1}$ and $\mathbf{H}$. The dashed vectors $\mathbf{n}_1$ and $\mathbf{n}_2$ represent the surface directors *after* the switching on of $\mathbf{H}$. β' is the angle between $\mathbf{n}_1$ and $\mathbf{H}$.

To characterize the NLC patterns we use both a transmitted-light technique and a reflectometric method. In the transmitted-light apparatus, a white light beam is polarized by a polarizer that makes an angle α_P with the magnetic field; then the light beam impinges on the NLC layer and crosses an analyzer at an angle α_A with the magnetic field. The transmitted light is collected by an objective and the image of the NLC layer is focused on a CCD camera (orthoscopic technique).

The reflectometric apparatus and the measurement method have been described in detail in reference [8] and thus, we summarize here only the main features. A 5 mW He-Ne laser beam is polarized by a polarizer that makes an angle α_P with the magnetic field and impinges at almost normal incidence on the NLC layer. To separate the laser beams reflected from the various interfaces, we make the cell with two mylar spacers of different thicknesses (130 μm and 260 μm), giving a wedge angle of 0.5°. The glass plates, too, are wedge shaped with a wedge angle of 0.4°. The laser beam reflected from the first SiO-NLC interface ($z = 0$) passes through a crossed analyzer ($\alpha_A = \alpha_P + \pi/2$) and its intensity I is measured by a photodetector. I is only sensitive to the director alignment in an interfacial layer of thickness $\delta \approx \lambda/2\pi$ (λ = optical wavelength) close to the first SiO-NLC interface. According to the theoretical analysis given in [8], if $\lambda/2\pi$ is much smaller than the characteristic thickness ξ of the director distortion, the intensity I is $I = I_0 \sin^2 [2(\alpha_P - \beta)]$, where I_0 can be measured by setting $\alpha_P = \beta + \pi/4$. A small rotation $\Delta\phi_S = \beta' - \beta \ll 1$ (see Fig. 2) of the director at the first surface produces the intensity variation $\Delta I = (\partial I/\partial\beta)\,\Delta\phi_S$. By setting $\alpha_P = \beta - \pi/8$, we find:

$$\Delta I = 2I_0 \Delta\phi_S. \tag{2.1}$$

When the magnetic field is switched on, a director distortion occurs in the NLC and the surface elastic torque $K_{22}\mathrm{d}\phi/\mathrm{d}z$ (K_{22} = twist elastic constant) induces a rotation $\Delta\phi_S(t)$ of the director at the surface. In our experimental conditions, the director rotation at the maximum magnetic field ($H = 7.7$ kG) is small ($\Delta\phi_S < 10^{-2}$) and the surface viscosity is completely negligible [9]. Thus, $\Delta\phi_S(t)$ satisfies the boundary equation [1]:

$$\Delta\phi_S(t) \approx \frac{K_{22}}{W_a} \left.\frac{\mathrm{d}\phi}{\mathrm{d}z}\right|_{z=0}, \tag{2.2}$$

where W_a is the azimuthal anchoring coefficient [10]. From (2.1) and (2.2), we find:

$$\left.\frac{d\phi}{dz}\right|_{z=0} = \frac{W_a}{K_{22}}\frac{\Delta I}{2I_0}. \tag{2.3}$$

Therefore, from a $\Delta I-$measurement one obtains the first derivative of $\phi(z)$ at the lower interface.

2.2. Observed NLC Patterns. — Figures 3 show the transmitted image of a small portion of the NLC layer at different times t after switching on a magnetic field ($H = 7.7$ kG, $\beta = 78°$). The NLC layer is observed between nearly parallel polarizers. Figure 3a shows the NLC layer before the magnetic field was switched on ($t = 0$). Because of the initial $\pi/2-$twist and the parallel polarizers, the NLC layer appears uniformly dark everywhere. A few seconds later, elliptical domains B nucleate at different sites in the NLC sample and grow slowly. Figure 3b shows a typical elliptical domain B, which is clearly visible due to its optical contrast with respect to the bounding region (domain A). At a later time, a new domain C nucleates at the borders of the NLC layer close to the mylar spacers and spreads throughout the observation region. Figure 3c shows the NLC layer at time $t = 79$ s, when all three domains are present in the observation region. Finally, in Figure 3d ($t = 170$ s), domain A has disappeared and domain B is collapsing inside domain C. These experimental observations indicate that the energy of textures A, B and C are ordered as follows: $E_C < E_B < E_A$.

The A-B interface is less sharp than the A-C and B-C interfaces. Moreover, when the magnetic field is switched off, the A-B interface vanishes and a monodomain of uniform twist remains, while the A-C and B-C interfaces remain stable or they shrink until they disappear. From these observations we conclude that the A-B interface has no topological charge, i.e. it consists of a continuous director deformation corresponding to a wall. In contrast, the A-C and B-C interfaces do have a topological charge and correspond to line defects. The A-C defect line has a regular curvature (see Fig. 3c) like a bulk line defect, whilst the B-C line is less regular and at some points it sticks to the surface of the glass plates (see Fig. 3d).

In order to characterize the nature of domains A, B and C more satisfactorily we measured the time dependence of the reflected-light intensity after switching on the magnetic field. Figure 4 shows a typical measurement when a magnetic field $H = 7.7$ kG is switched on at $t = 0$. Immediately after switching on the magnetic field (region (a) in Fig. 4), $\Delta I(t) < 0$; thus $d\phi/dz|_{z=0} < 0$ (see (2.3)). In transmitted light, we see a homogeneous domain A. After a time $t \approx 30$ s, $\Delta I(t)$ changes sign (region (b)). In transmitted light, we see that domain A is replaced by domain B everywhere after $t \approx 50$ s, when the reflected intensity in Figure 4 reaches an almost stationary positive value. If the $\beta-$angle is higher than a critical value $\beta_c = \beta_c(H)$, the transition from (a) to (b) in Figure 4 is nearly homogeneous, i.e. without nucleation of spatial domains. After 300 s (region (c)), $\Delta I(t)$ returns negative and $d\phi/dz|_{z=0}$ has the same sign as in (a). This regime corresponds to the occurrence of the domain C. At time $t \approx 400$ s, domain C has completely replaced domain B. The transition from (b) to (c) occurs always with the appearance of spatial domains and disclination lines. This means that domain B is metastable. Finally, in region (d), the magnetic field is turned off and the reflected light intensity relaxes toward the initial value.

In conclusion, domains A, B and C correspond to different bulk twisted textures. From the experimental observations, we believe that domain A corresponds to an unstable texture with slow relaxation dynamic and negative value of the surface director twist ($d\phi/dz|_{z=0} < 0$). Domain B corresponds to a metastable texture with $d\phi/dz|_{z=0} > 0$ and, finally, domain C corresponds to a stable texture with $d\phi/dz|_{z=0} < 0$.

a)

b)

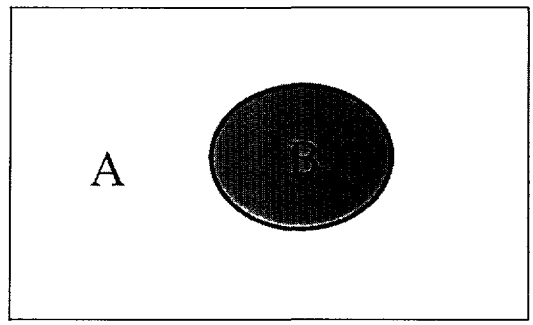

b')

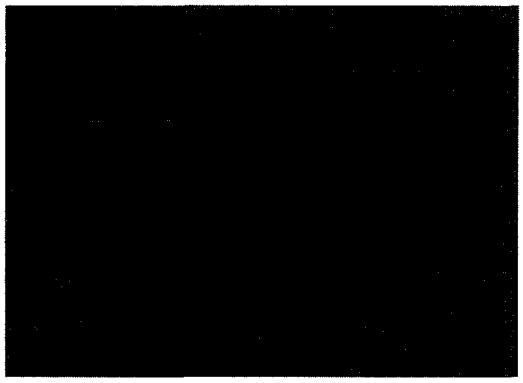

c)

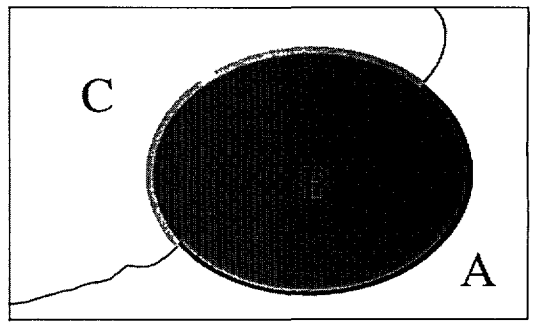

c')

Fig. 3. — Cell in transmitted light at different times t_H after the switching on of a 7.7 kG magnetic field at an angle $\beta = 78°$. The polarizers are parallel with angles $\alpha_P = \alpha_A = 75°$. (a) $t_H = 0$. (b) $t_H = 67$ s. The A-B interface is a wall. (c) $t_H = 79$ s. The A-C and B-C interfaces are defect lines. (d) $t_H = 170$ s. Domain A has disappeared. The B-C defect line remains stuck at some points of the surface.

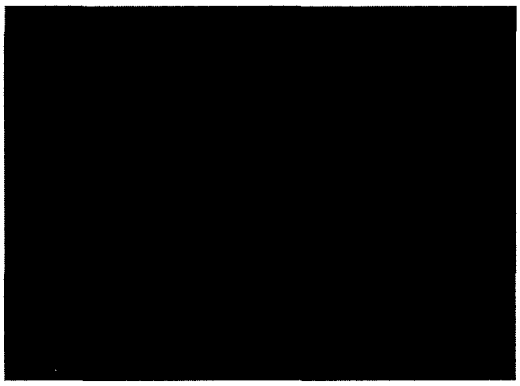

d)

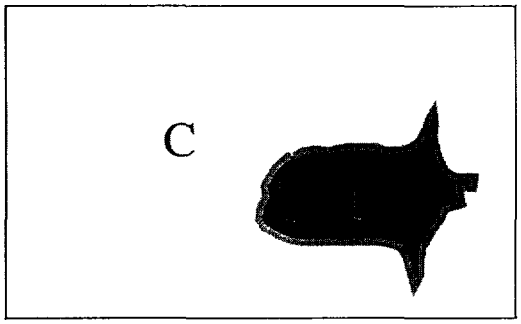

d')

Fig. 3. — *(Continued)*

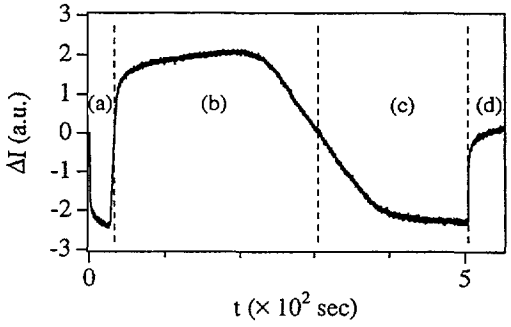

Fig. 4. — Reflected light intensity variation ΔI between crossed polarizers *versus* time t after the switching on of a magnetic field $H = 7.7$ kGauss at an angle $\beta = 80.5°$. In the parts (a), (b) and (c) the magnetic field is on, while in the part (d) is off.

In Section 3, we will analyse the possible stationary and dynamical transient patterns in our special geometry.

3. Theoretical Analysis of the NLC Stationary and Dynamical Textures

Our reflectometric method needs the use of a wedge NLC sample to pick-out the laser beam reflected from the lower surface. The wedge angle is very small ($\approx 10^{-2}$ rad) and the relative thickness variation over the observation region of diameter approximately 1 mm is $\Delta d/d \approx 5\%$ ($d = 195$ μm). Therefore the wedge does not appreciably affect the physical properties of the system. To check this important point, we performed a control experiment by using a planar NLC layer. The physical behaviour of this planar layer was found to be equivalent to that of the wedge sample. Thus, in our theoretical analysis, we can disregard the wedge angle. Furthermore, in our experiment, the extrapolation length [1] $b = K_{22}/W_a$ is much smaller than the magnetic coherence length:

$$\xi = \sqrt{\frac{K_{22}}{\chi_\alpha}} \frac{1}{H}, \tag{3.1}$$

where χ_α is the diamagnetic anisotropy. In particular, $b/\xi \approx 10^{-2}$ at the maximum magnetic field $H = 7.7$ kG. Therefore the theoretical analysis of the static and dynamic bulk director-field can be made by assuming strong anchoring conditions ($b/\xi \to 0$).

3.1. STATIONARY DIRECTOR TEXTURES. — Let us consider a NLC cell with two plane parallel surfaces: surface 1 at $z = 0$ and surface 2 at $z = d$. In this Section we are interested in finding out the stationary configurations of the director when the director-field is assumed to be homogeneous in the $x - y$ plane. We assume that the director lies everywhere in the $x - y$ plane and that its orientation is a function of z only. $\phi(z)$ is the angle between the director and the $\hat{\mathbf{x}}$-axis parallel to $\mathbf{H}$. The easy angles at the 1 and 2−surfaces are β and $\beta + \pi/2$, respectively (see Fig. 2). In the absence of the magnetic field, the director goes from surface 1 to surface 2 by making a uniform twist distortion $\phi_0(z)$:

$$\phi_0(z) = \beta + \frac{\pi}{2}\,\frac{z}{d}. \tag{3.2}$$

The free energy per unit surface area is:

$$E = \int_0^d F\,\mathrm{d}z, \tag{3.3}$$

where F is the free energy density given by [1]:

$$F = \frac{K_{22}}{2}\left(\frac{\mathrm{d}\phi}{\mathrm{d}z}\right)^2 - \frac{\chi_\alpha}{2}H^2\cos^2\phi. \tag{3.4}$$

By minimizing the total free energy (3.3) we find:

$$\xi^2\frac{\mathrm{d}^2\phi}{\mathrm{d}z^2} - \frac{\sin(2\phi)}{2} = 0, \tag{3.5}$$

with the boundary conditions:

$$\phi(0) = \beta, \tag{3.6a}$$

$$\phi(d) = \beta + \frac{\pi}{2} \tag{3.6b}$$

The first integral of equation (3.5) has the form:

$$\frac{\mathrm{d}\phi}{\mathrm{d}z} = \pm\frac{1}{\xi}\sqrt{C_0 - \frac{1}{2}\cos 2\phi}, \tag{3.7}$$

where C_0 is a constant. Here we restrict our attention to the range $\pi/4 \leq \beta \leq \pi/2$. For $\xi > \xi_{c_{(I)}}$ (see (3.8)), the director angle $\phi(z)$ is a monothonic function everywhere as shown in Figure 5a. By increasing the amplitude of the magnetic field, an inversion point ($\mathrm{d}\phi/\mathrm{d}z = 0$) appears if $\xi \leq \xi_{c_{(I)}}$ and the ϕ−profile has the form shown in Figure 5b. We indicate the corresponding texture as texture (I). At the inversion point, $\phi = \phi_{\max}$ and $\mathrm{d}\phi/\mathrm{d}z = 0$; then constant C_0 is given by: $C_0 = (1/2)\cos(2\phi_{\max_{(I)}})$. The characteristic coherence length $\xi_{c_{(I)}}$ corresponding to $\phi_{\max_{(I)}} = \beta + \pi/2$ is determined by the integral:

$$\frac{d}{\xi_{c_{(I)}}} = \int_\beta^{\beta+\pi/2} \frac{\mathrm{d}\phi'}{\sqrt{-\frac{1}{2}(\cos 2\beta + \cos 2\phi')}}. \tag{3.8}$$

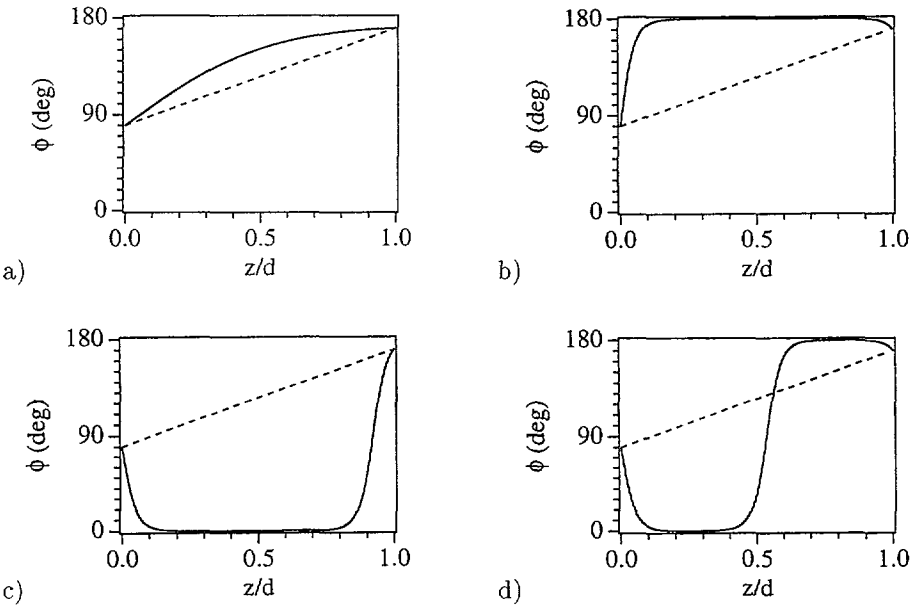

Fig. 5. — (a) $\phi(z)$ profile *versus* z/d for $\beta = 80°$ and $\xi/d = 3.2 \times 10^{-1}$ (solid line). (b) Texture (I) profile *versus* z/d for $\beta = 80°$ and $\xi/d = 3.2 \times 10^{-2}$ (solid line). (c) Texture (II) profile *versus* z/d for $\beta = 80°$ and $\xi/d = 3.2 \times 10^{-2}$ (solid line). (d) Texture (III) profile *versus* z/d for $\beta = 80°$ and $\xi/d = 3.2 \times 10^{-2}$ (solid line). The dashed lines in Figures (a-d) represent the initial uniform twist.

For $\xi < \xi_{c_{(I)}}$, $\phi_{\max_{(I)}}$ is determined by dividing the z-interval in Figure 5b in two parts with $d\phi/dz > 0$ for $0 \leq z \leq d_1$ and $d\phi/dz < 0$ for $d_1 \leq z \leq d$, respectively (d_1 is defined as: $\phi(d_1) = \phi_{\max_{(I)}}$). By exploiting (3.7) we find:

$$\int_{\beta}^{\phi_{\max_{(I)}}} \frac{d\phi'}{\sqrt{\frac{1}{2}(\cos 2\phi_{\max_{(I)}} - \cos 2\phi')}} - \int_{\phi_{\max_{(I)}}}^{\beta+\pi/2} \frac{d\phi'}{\sqrt{\frac{1}{2}(\cos 2\phi_{\max_{(I)}} - \cos 2\phi')}} = \frac{d}{\xi} \tag{3.9}$$

Then, the $\phi(z)$ profile of texture (I) is obtained by:

$$\begin{cases} \dfrac{z}{\xi} = \displaystyle\int_{\beta}^{\phi} \frac{d\phi'}{\sqrt{\frac{1}{2}(\cos 2\phi_{\max_{(I)}} - \cos 2\phi')}} & \text{for} \quad 0 \leq z \leq d_1, \\ \dfrac{z - d_1}{\xi} = -\displaystyle\int_{\phi_{\max_{(I)}}}^{\phi} \frac{d\phi'}{\sqrt{\frac{1}{2}(\cos 2\phi_{\max_{(I)}} - \cos 2\phi')}} & \text{for} \quad d_1 \leq z \leq d. \end{cases} \tag{3.10}$$

For large-enough magnetic fields, when $\xi < \xi_{c_{(II)}} = \xi_{c_{(III)}}$ ($\xi_{c_{(II)}}$ is given by (3.11)), two other stationary textures are possible: texture (II) and texture (III). Texture (II) is shown in Figure 5c. The director starts from β on surface 1, with a negative surface derivative, then reaches a minimum $\phi_{\min_{(II)}}$, and then goes to $\beta + \pi/2$ on surface 2 ($z = d$). The calculus of $\phi_{\min_{(II)}}$ and $\phi(z)$ for texture (II) is analogous to that made previously for texture (I).

Texture (III) is shown in Figure 5d. The bulk director orientation goes from β to $\phi_{\min_{(III)}} \approx 0$ with a negative $d\phi/dz|_{z=0}$ and from $\phi_{\min_{(III)}} \approx 0$ to $\phi_{\max_{(III)}} \approx \pi$ by making a twist π-wall. By substituting $d\phi/dz = 0$ in (3.7) at the two inversion points of texture (III), we

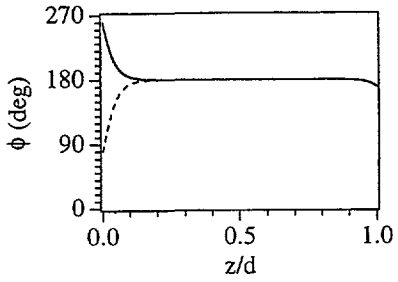

Fig. 6. — Texture (IV) profile (solid line) and texture (I) profile (dashed line) *versus* z/d for $\beta = 80°$ and $\xi/d = 3.2 \times 10^{-2}$

find: $C_0 = (1/2)\ \cos(2\phi_{\min_{(III)}}) = (1/2)\ \cos(2\phi_{\max_{(III)}})$; thus $\phi_{\max_{(III)}} = \pi - \phi_{\min_{(III)}}$. Other possible solutions, namely $\phi_{\max_{(III)}} = \pi + \phi_{\min_{(III)}}$ are not allowed for a continuous function $\phi(z)$ satisfying (3.5). The calculation of $\phi_{\min_{(III)}}$ and $\phi(z)$ for texture (III) is analogous to the previous one for texture (I).

To calculate threshold $\xi_{c_{(II)}}$, we consider texture (II) in Figure 5c and imagine decreasing the magnetic field amplitude (increasing ξ). $\phi_{\min}$ increases until it reaches the value $\phi_{\min} = \pi/2 - \beta$, for $\xi = \xi_{c_{(II)}}$. At $\xi = \xi_{c_{(II)}}$, a maximum of $\phi(z)$ appears at the second interface ($z = d$). Indeed, $\cos[2(\beta + \pi/2)] = \cos[2(\pi/2 - \beta)] = 2C_0$, that gives $\mathrm{d}\phi/\mathrm{d}z = 0$ in (3.7). Textures (II) and (III) coincide at the threshold field; thus, $\xi_{c_{(II)}} = \xi_{c_{(III)}}$, where $\xi_{c_{(II)}}$ is given by:

$$-\int_{\beta}^{\pi/2-\beta} \frac{\mathrm{d}\phi'}{\sqrt{-\frac{1}{2}(\cos 2\beta + \cos 2\phi')}} + \int_{\pi/2-\beta}^{\beta+\pi/2} \frac{\mathrm{d}\phi'}{\sqrt{-\frac{1}{2}(\cos 2\beta + \cos 2\phi')}} = \frac{d}{\xi_{c_{(II)}}} \tag{3.11}$$

For $\beta = \pi/4$, textures (I) and (II) are symmetrical with respect to the changes $\phi_{(I)}(z) \rightarrow \pi - \phi_{(II)}(z)$ and $z \rightarrow d - z$. For $0 \leq \beta \leq \pi/4$, the same reasoning applies but with textures (I) and (II) interchanged.

For $\xi < \xi_{c_{(II)}}$, all three textures are stationary solutions for the director-field. By continuously modifying the $\phi(z)$ profile, we can transform one of these three textures into one of the other two. The solid line in Figure 6 shows another possible stationary texture (texture (IV)), while the dashed line shows texture (I). Texture (IV) is made possible because of the planar homogeneous surface alignment of the director and because of the equivalence of the $\phi = \beta$ and $\phi = \beta + \pi$ surface states. Texture (IV) is allowed for any value of ξ and cannot be transformed continuously into any of the previous textures. This means that, if both texture (I) and texture (IV) are present in the NLC layer, a π-discontinuity separates texture (I) from texture (IV), i.e. a 1/2-twist-line defect must be present. The same conclusions apply to interfaces (II)-(IV) and (III)-(IV).

3.2. Stability of the Stationary Textures

3.2.1. Global Stability. — The free energy per unit area E is:

$$E = \int_0^d F\ \mathrm{d}z = \int_{\beta}^{\beta+\pi/2} \frac{F}{\frac{\mathrm{d}\phi}{\mathrm{d}z}}\ \mathrm{d}\phi, \tag{3.12}$$

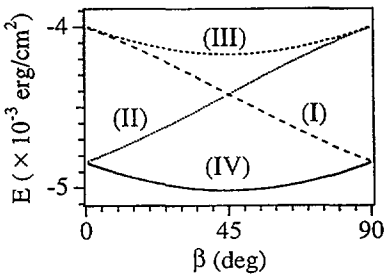

Fig. 7. — Surface free energy density E *versus* the angle β of the four stationary textures for $\xi = 7.7 \times 10^{-4}$ cm, $d = 1.95 \times 10^{-2}$ cm and $K_{22} = 3.27 \times 10^{-7}$ dyne [17].

Using (3.7), we obtain:

$$F = \frac{1}{2}\chi_\alpha H^2 \left(C_0 - \frac{3}{2} + 2\sin^2\phi \right). \tag{3.13}$$

Since the sign of $\mathrm{d}\phi/\mathrm{d}z$ can change for different intervals of the $z-$axis (see (3.7)), the integral in (3.12) must be evaluated separately for these intervals. Therefore E can be written as the sum of the free energies E_i of each interval that are:

$$\begin{cases} E_i = \pm \displaystyle\int_{\phi_i}^{\phi_i'} e(\phi)\ \mathrm{d}\phi \\ e(\phi) = \dfrac{1}{2}\dfrac{K_{22}}{\xi}\ \dfrac{C_0 - (3/2) + 2\sin^2\phi}{\sqrt{C_0 - (1/2) + \sin^2\phi}}, \end{cases} \tag{3.14}$$

where $e(\phi) = F/|\mathrm{d}\phi/\mathrm{d}z|$, and ϕ_i and ϕ_i' are the director angles at the extremes of the i-th interval. For texture (I) we obtain:

$$\begin{cases} E_{(\mathrm{I})} = \displaystyle\int_{\beta}^{\phi_{\max_{(\mathrm{I})}}} e_{(\mathrm{I})}(\phi)\ \mathrm{d}\phi - \int_{\phi_{\max_{(\mathrm{I})}}}^{\beta+\pi/2} e_{(\mathrm{I})}(\phi)\ \mathrm{d}\phi \\ e_{(\mathrm{I})}(\phi) = \dfrac{1}{2}\dfrac{K_{22}}{\xi}\ \dfrac{-\sin^2\phi_{\max_{(\mathrm{I})}} + 2\sin^2\phi - 1}{\sqrt{\sin^2\phi - \sin^2\phi_{\max_{(\mathrm{I})}}}} \end{cases} \tag{3.15}$$

The calculation of the other free energies $E_{(\mathrm{II})}$, $E_{(\mathrm{III})}$ and $E_{(\mathrm{IV})}$ follows that of texture (I).

Figure 7 shows $E_{(\mathrm{I})}$, $E_{(\mathrm{II})}$, $E_{(\mathrm{III})}$, $E_{(\mathrm{IV})}$ *versus* the angle β. The energy of texture (III) is always largest; the energy of texture (IV) is always the smallest. For $\beta = 45°$, the energies of textures (I) and (II) coincide, as expected.

3.2.2. Local Stability. — According to the Jacobi criterion [11], a stationary solution $\phi(z)$ of the problem $\delta E = \delta \int_0^d F\ \mathrm{d}z = 0$ is a local minimum if and only if $\partial^2 F/\partial\dot{\phi}^2 = F_{\dot\phi\dot\phi} > 0$ ($\dot\phi = (\mathrm{d}\phi)/(\mathrm{d}z)$) and if any solution $u(z)$ of the Jacobi equation

$$\left(F_{\phi\phi} - \frac{\mathrm{d}}{\mathrm{d}z} F_{\dot\phi\phi} \right) u - \frac{\mathrm{d}}{\mathrm{d}z}\left(F_{\dot\phi\dot\phi}\dot{u} \right) = 0 \tag{3.16}$$

($\dot{u} = (\mathrm{d}u/\mathrm{d}z)$ and $F_{\phi\phi} = \partial^2 F/\partial\phi^2$) which is null at $z = 0$ ($u(0) = 0$) is never zero in the open interval $]0, d]$. With F given by (3.4), we find:

$$F_{\dot\phi\phi} = K_{22} > 0, \tag{3.17}$$

and the Jacobi equation (3.16) becomes:

$$\xi^2 \ddot{u} - \cos(2\phi(z))u = 0. \tag{3.18}$$

One immediately has one solution $u_1 = \dot{\phi}(z)$, where $\phi(z)$ is the solution of (3.5) to be tested. Thus texture (III) is not a minimum because it has two extrema, and therefore two zeros of u_1 inside the integration range (*conjugate points*). Furthermore $\phi_{(III)}(z)$ is not a maximum, because $F_{\dot{\phi}\dot{\phi}} > 0$. Thus, texture (III) corresponds to a saddle point. To prove the local stability of the other stationary solutions we must use a numerical method.

Equation (3.18) is a linear and homogeneous second order equation: if $u_0(z)$ is a single solution that satisfies the condition $u_0(0) = 0$, the general solution that will satisfy this condition is $u(z) = Au_0(z)$, with A an arbitrary constant. Obviously, if $u_0(z) \neq 0$ in the open interval $]0, d]$, then $u(z) \neq 0$ in the same interval. Therefore we can restrict our study to the single solution $u_0(z)$ that satisfies the two initial conditions:

$$u_0(0) = 0, \tag{3.19a}$$

$$\dot{u}_0(0) = 1. \tag{3.19b}$$

We have solved equation (3.18) numerically with conditions (3.19a) and (3.19b) for the textures $\phi_{(I)}(z)$, $\phi_{(II)}(z)$ and $\phi_{(IV)}(z)$ with different values of β and H. $u_0(z)$ is never zero in the interval $]0, d]$, and, thus, textures (I), (II) and (IV) are local minima. The analysis of the free energies of textures (I), (II) and (IV) gives $E_{(IV)} < E_{(I)} < E_{(II)}$ for $\pi/4 < \beta < \pi/2$. Thus textures (I) and (II) are metastable textures, and instead, texture (IV) is the absolutely stable texture. Indeed, we can show that any other possible solution of (3.5) has free energy higher than $E_{(IV)}$. Thus, texture (IV) should be reached from the system at the equilibrium. However, according to the analysis in Section 3.1, texture (IV) needs the nucleation of a 1/2 disclination line, while textures (I) and (II) can be reached through a continuous deformation of the director-field.

3.3. The Transient Homogeneous Relaxation. — The presence of an initial uniform twist in the nematic layer makes the dynamical relaxation of the system somewhat complex if $0 < \beta < \pi/2$. In this case, in the initial state, there exists a point z^* in the NLC layer given by:

$$z^* = 2d\,\frac{(\pi/2) - \beta}{\pi} \tag{3.20}$$

where the director makes the angle $\phi(z^*) = \pi/2$ with the magnetic field. For $z < z^*$, $\phi(z) < \pi/2$ and the magnetic torque tends to orient the director parallel to $\mathbf{H}$ ($\phi = 0$). For $z > z^*$, $\phi(z) > \pi/2$ and the magnetic torque tends to orient the director antiparallel to $\mathbf{H}$ ($\phi = \pi$). This means that the magnetic field generates a transient distortion which is qualitatively of the same form as texture (III), but having the $\pi-$wall close to position z^*. The director angle $\phi(z, t)$ after switching on the magnetic field can be obtained by numerical integration of the Leslie-Enricksen hydrodynamic equation. A detailed analysis of this dynamical behaviour has been given by us in reference [4], where the homogeneous relaxation regime was investigated. Here we only report on the principal features that are relevant in the analysis of the inhomogeneous case. After a characteristic time $\tau_R \approx \gamma_1/(\chi_\alpha H^2)$ (γ_1 is the orientational viscosity coefficient), the director field relaxes toward an intermediate state having a $\pi-$wall at $z = z^*$. This $\pi-$wall texture is shown in Figure 8. τ_R is of the order of few seconds for the NLC 5CB if $H \approx 1$ kG. If $3\xi < z^* < d/2 - 3\xi$, this texture is nearly stationary and the $\pi-$wall slowly approaches surface $z = 0$ with the relaxation time:

$$\tau_W \approx \frac{\tau_R}{4 \tan \dfrac{\beta}{2}} \exp\left[\left(1 - \frac{2\beta}{\pi}\right)\frac{d}{\xi}\right]. \tag{3.21}$$

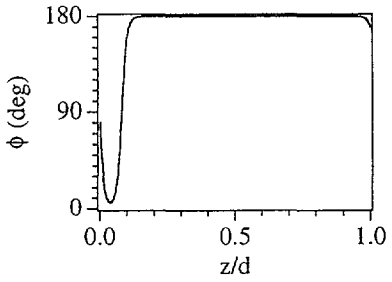

Fig. 8. — Director angle $\phi(z)$ of the dynamical $\pi-$wall texture at time $t = 10$ s after the magnetic field has been switched on. $H = 7.7$ kG, $\beta = 80°$ and the material parameters are $K_{22} = 3.27 \times 10^{-7}$ dyne [17], $\chi_\alpha = 1.14 \times 10^{-7}$ [18] and $\gamma_1 = 0.72$ poise [19] ($\xi/d = 1.12 \times 10^{-2}$).

Once the $\pi-$wall approaches $z = 0$, the system quickly relaxes toward texture (I). An analogous behaviour occurs if $d/2 - 3\xi < z^* < d - 3\xi$ ($\beta < \pi/4$). In such a case, the $\pi-$wall approaches $z = d$ and relaxes toward texture (II). The exponential factor in (3.21) plays a very important role in determining the qualitative and quantitative behaviour of our system. Because of this factor, the τ_W-time depends strongly on the director angle β and on the magnetic coherence length ξ. In particular, $\tau_W \gg \tau_R$ in the high-magnetic-field regime ($\xi \ll d$).

3.4. CONCLUSIONS. — The analysis above allows us to understand the nature of the optical domains that were observed in the experiment (Sect. 2.2). First, we summarize the properties found for each observed domain: domain A is unstable and it relaxes toward domains B and C. Domain B relaxes toward domain C. The relaxation toward texture C occurs always through nucleation of disclination lines, whilst the relaxation toward texture B occurs without nucleation of disclination lines. Furthermore, the transition to texture B can occur either homogeneously or inhomogeneously, depending on the H and $\beta-$values. In particular, a homogeneous relaxation is always seen when the $\beta-$angle exceeds a critical value $\beta_c(H)$. In both these cases (homogeneous and inhomogeneous) a strong variation of the reflected light intensity ((a)-(b) transition in Fig. 4) is observed. The homogeneous regime has been extensively investigated in [4], and the characteristic time for the (a)-(b) transition in Figure 4 is in a good quantitative agreement with τ_W given in (3.21). Thus, domain A has to be identified as the $\pi-$wall texture shown in Figure 8, whilst domain B must correspond to texture (I) for $\pi/4 < \beta < \pi/2$ and to texture (II) for $0 < \beta < \pi/4$. In principle, both textures (I) and (II) should coexist for $\beta = \pi/4$. However, the observation of this co-existence requires β to be set accurately to $\beta = \pi/4$ and we have not made a detailed investigation on this point. Domain C corresponds to the equilibrium texture and, thus, it must consist of the stationary state of minimum free energy. Furthermore it always appears coupled with a defect line which separates this domain by domains A and B. We can, then, conclude that domain C consists of texture (IV). All these conclusions are in agreement with the signs of $d\phi/dz|_{z=0}$ that are measured by means of the reflectometric apparatus. Texture (III) is a saddle point of the free energy and it never appears, due to the initial conditions, except for the very special case $\beta = \pi/4$ where $z^* = d/2$ and texture (III) coincides with the $\pi-$wall dynamic texture.

4. Structure and Form of the Interfaces

Figures 9a, b show the cell at time $t_H = 120$ s after switching on a magnetic field $H = 7.7$ kG for $\beta = 75°$. In Figure 9a one can see one dark region corresponding to domain B (texture (I))

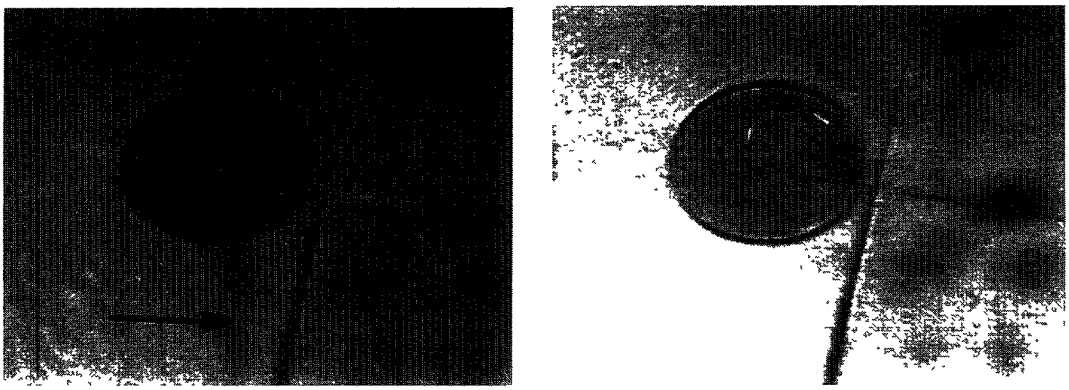

a) b)

Fig. 9. — Cell in transmitted light at a time $t_H = 120$ s after switching on the magnetic field ($H = 7.7$ kG, $\beta = 75°$). The arrow denotes the magnetic field orientation. The local thickness is $d = 195 \pm 5$ μm. (a) The polarizers are parallel: $\alpha_P = \alpha_A = 75°$. The dark and white regions represent texture (I) and π−wall texture, respectively. (b) The polarizers are crossed: $\alpha_P = 75°$ and $\alpha_A = 165°$. The applied magnetic field is parallel to the long axis of the ellipses.

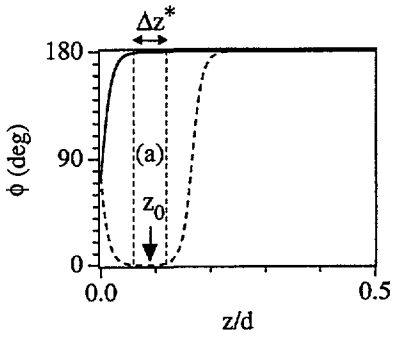

Fig. 10. — The π−wall texture (dashed line) and texture (I) (solid line) for $\beta = 75°$ and $H = 7.7$ kG ($\xi/d = 1.12 \times 10^{-2}$). In region ($a$) of width Δz^* around z_0 the two texture angles differ by π.

bounded by a white region corresponding to the domain A (π-wall texture). In Figure 9a the polarizer is approximately parallel to the analyzer. The contrast between the two regions is due to the non-adiabaticity of the transmitted light and to the different sign of the twist distortion in the two regions [12]. In Figure 9b, the polarizers are crossed approximately and the interface between the two regions is more visible. Domain B has an elliptical shape, with the long axis parallel to the magnetic field. To explain the ellipticity of domain B, we must analyze the shape of the director-field close to the interface between the two regions shown in Figure 9. Figure 10 shows the z−dependence of the director angle in texture (I) (solid line) and in the π−wall texture (dashed line) for $\beta = 75°$ and $H = 7.7$ kG. We see that there is a z−interval around a characteristic depth z_0 ((a) in Fig. 10) where the director angles of the two textures differ by π approximatively. Therefore, to pass from one texture to the other, the director must rotate by π in this z−interval. This rotation is expected to occur within a characteristic length of the order of the magnetic coherence length ξ. In Figure 11 we show a $z = z_0$ section

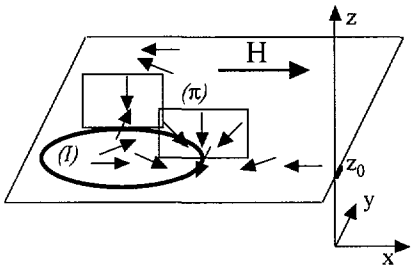

Fig. 11. — Schematic representation of the elastic distortion at the interface between texture (I) (inside the ellipsis) and the π−wall texture in the plane $z = z_0$. Along the long axis of the ellipsis, parallel to **x**, the only possible distortions are splay-bend. Along the short axis of the ellipsis parallel to **y** the two possible distortions are a splay-bend distortion in the $z = z_0$ plane or a twist distortion outside the $z = z_0$ plane.

of the NLC layer with the possible distortion across the interface. By crossing the (π-wall)-(I) interface along the **x**-axis we always have a splay-bend distortion either in the $z = z_0$ plane or in a plane parallel to $y = 0$. If we cross the (π-wall)-(I) interface along the **y**-axis we have two possibilities: (1) a twist distortion with the director escaped from the $z = z_0$ plane or (2) a splay-bend distortion in the $z = z_0$ plane. In case (1), the director in the centre of the wall is parallel to **z** while, in case (2), it remains in a plane parallel to the surface. Note that the director at the interface must be parallel to the surface (planar anchoring). This means that, if distortion (1) occurs, the director must rotate from the z−axis toward the easy axis in a region close to the surface of thickness $\bar{\xi}$: a splay-bend distortion must be present in this interfacial region. $\bar{\xi} = \sqrt{\bar{K}/\chi_\alpha}/H$ is the magnetic coherence length that is related to the splay-bend distortion, where $\bar{K}$ is an average of the splay and bend elastic constants ($\bar{K} > K_{22}$). In contrast, in case (2), the director remains in the film plane and, thus, it can reach the easy axis by means of a twist distortion. We can roughly estimate the energies $\gamma_{(1)}$ and $\gamma_{(2)}$ per unit of length of the (π-wall)-(I) interface in the case of the twist wall and splay-bend wall. respectively, as:

$$\gamma_{(1)} = \frac{K_{22}}{\xi^2}(\xi \Delta z^*) + \frac{\bar{K}}{\bar{\xi}^2}\bar{\xi}^2, \tag{4.1a}$$

$$\gamma_{(2)} = \frac{\bar{K}}{\bar{\xi}^2}(\bar{\xi} \Delta z^*) + \frac{K_{22}}{\xi^2}\xi^2, \tag{4.1b}$$

where Δz^* is the wall depth (see Fig. 10). For sufficiently high magnetic fields, $\Delta z^* \approx z^* = 2d(\pi/2 - \beta)/\pi > \xi$ and $\gamma_{(1)} < \gamma_{(2)}$. Therefore, a twist distortion with line tension $\gamma \approx \gamma_{(1)}$ is present if the wall is parallel to **H**, whilst a splay-bend distortion with $\gamma \approx \gamma_{(3)} = \bar{K}\Delta z^*/\bar{\xi}$ is present if the wall is orthogonal to **H**. Such a rough analysis allows us to obtain an estimate of ellipticity e of domain B. By analogy with the case of the Freedericksz transition, we can assume [13] :

$$\gamma(\theta) = \gamma_{(3)}\sqrt{\frac{\gamma_{(1)}^2}{\gamma_{(3)}^2}\cos^2\theta + \sin^2\theta}, \tag{4.2}$$

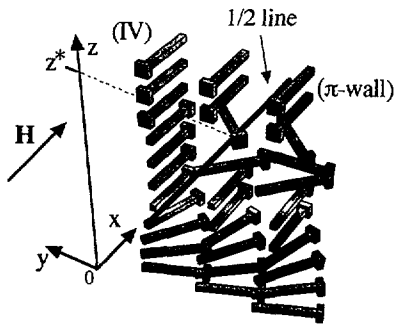

Fig. 12. — Schematic view of the 1/2 disclination line at the (IV)-(π-wall) interface. The 1/2 line is positioned at $z = z^*$, where z^* is the position of the π-wall.

where θ is the angle between **H** and the wall. According to Brochard [13], $\Gamma = \int \gamma(\theta) \mathrm{d}S$ is minimum if

$$e = \frac{\gamma_{(1)}}{\gamma_{(3)}} = \frac{K_{22}\Delta z^*/\xi + \bar{K}}{\bar{K}\Delta z^*/\bar{\xi}} \tag{4.3}$$

Using the experimental values [14] $K_{22} = 3.27 \times 10^{-7}$ dyne and $\bar{K} = 7.8 \times 10^{-7}$ dyne and the same geometric parameters as in Figure 9b ($\beta = 75°$, $d = 1.95 \times 10^{-2}$ cm, $\xi/d = 1.12 \times 10^{-2}$, $\bar{\xi}/d = 1.73 \times 10^{-2}$) we obtain $\Delta z^* = 3.25 \times 10^{-3}$ cm and $e = 0.75$. This theoretical value of the ellipticity e is in reasonable agreement with the experimental value $e = 0.8$ that is obtained from Figure 9.

Now we can explain why the 1/2 line defect for the (I)-(IV) interface (B-C interface in Fig. 3d) remains stuck at some points on the glass surface. When the 1/2 bulk defect reaches the interface between the π-wall texture and texture (I), to minimize the elastic energy of the new interface, the 1/2 core is positioned in z^*, i.e. at the $z-$position of the π-wall where $\phi(z^*) = \pi/2$. This can be understood by looking at Figure 12. Therefore, when we have the (π-wall)-(I) transition, z^* goes toward the surface $z = 0$ and the bulk line follows this displacement. When texture (I) is formed, point z^* approaches the surface ($z^* \approx \xi$) and the 1/2 defect can remain stuck at some points on the surface, as in Figure 3d.

5. Dynamic Behaviour of the Interfaces

5.1. Line Velocities. — The interfaces (disclination lines or walls) between different textures move slowly with time. According to the standard theory [15], the displacement of a line or wall is due to a generalized force F_{gen} per unit of length that acts on the interface. For a straight line, this force is given by the difference ΔE of the surface free energy densities of the two adjacent textures. Futhermore, we can assume $F_{\mathrm{gen}} = \gamma_{\mathrm{eff}} v$ [16], where γ_{eff} is a sort of effective viscosity coefficient that can also depend on v. Thus, velocity v of the interface is:

$$v = \frac{\Delta E}{\gamma_{\mathrm{eff}}} \tag{5.1}$$

The free energies of texture (I) and (IV) can be obtained by using the theoretical procedure outlined in Section 3.2.1 (see Fig. 7). The calculation of the free energy of the dynamical $\pi-$wall texture requires a preliminary numerical integration of the Leslie-Enricksen hydrodynamic equations.

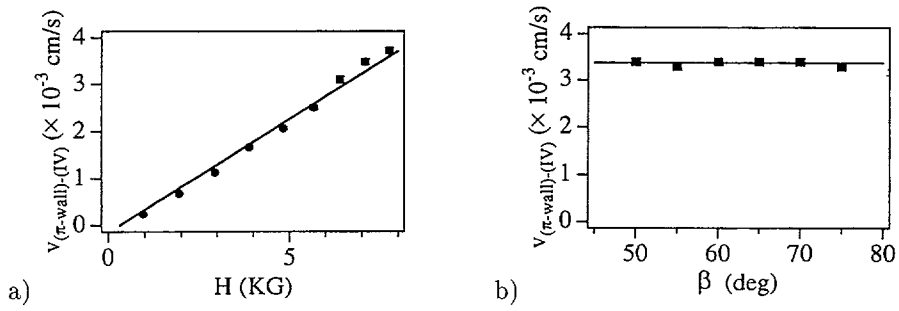

Fig. 13. — Velocity $v_{(\pi-\text{wall})-(\text{IV})}$ of the $(\pi$ − wall) − (IV) interface *versus* H for $\beta = 45°$ (a) and *versus* β for $H = 7.7$ kG (b). The points represent the experimental values, the solid lines are the best fit to 5.1 with a constant viscosity coefficient $\gamma_{\text{eff}} = 0.42$ poise/cm.

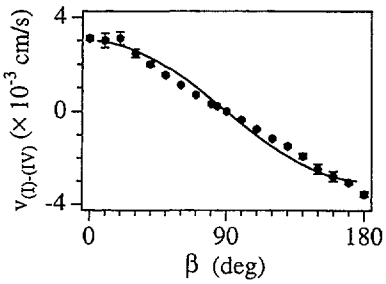

Fig. 14. — Velocity $v_{(\text{I})-(\text{IV})}$ of the (I)-(IV) interface *versus* β for $H = 7.7$ kG. The points represent the experimental values, the solid line the best to 5.1 with a constant viscosity coefficient $\gamma_{\text{eff}} =$ 0.5 poise/cm.

The points in Figure 13a show the experimental values of the velocity $v_{(\pi-\text{wall})-(\text{IV})}$ of the 1/2 twist bulk line between the π-wall texture (domain A) and texture (IV) (domain C) as a function of H for $\beta = 45°$. The experimental measurements refer to a disclination line that is much longer than the cell thickness. The points in Figure 13b represent velocity $v_{(\pi-\text{wall})-(\text{IV})}$ *versus* β for $H = 7.7$ kG. The observed dependence of $v_{(\pi-\text{wall})-(\text{IV})}$ on β and H can easily be understood by using a simple theoretical argument. First we note that the main difference between the $\phi(z)$ profiles of the two textures in Figures 6a and 8, is the presence of a $\pi-$wall. Therefore, ΔE can be roughly estimated as the energy per unit surface area of the $\pi-$wall that is proportional to $K_{22}(\pi/\xi)^2\xi$, i.e. linear in the magnetic field amplitude and independent of β, in good agreement with the experiment. This rough analysis is fully confirmed by an exact numerical calculation of the free energies of the different textures. The solid lines in Figures 13 represent the best fits to (5.1) obtained with a constant effective viscosity coefficient $\gamma_{\text{eff}_{(\pi-\text{wall})-(\text{IV})}} = 0.42$ poise/cm.

Figure 14 shows velocity $v_{(\text{I})-(\text{IV})}$ of the 1/2 defect line between texture (I) and texture (IV) *versus* the surface angle β for $H = 7.7$ kG. The solid line represents the best fit to (5.1) with $\gamma_{\text{eff}_{(\text{I})-(\text{IV})}} = 0.5$ poise/cm. This coefficient is a little larger than that of the $(\pi-$wall)-(IV) interface, since the (I)-(IV) interface is closer to the surface and, at some points, stuck to the surface.

The experimental analysis of the (π-wall)-(I) interface velocity is not possible over a large range of β and H values because this interface is only observed for a restricted range of values of H and β, as will be explained in the next Section. Therefore, we do not report experimental results concerning the dynamics of this kind of interface in the present paper. If $3\xi < z^* < d - 3\xi$, the free energy of the π-wall texture virtually coincides with that of texture (III) (see Fig. 7). According to the above analysis, the theoretical $\beta-$dependence of the velocity $v_{(\pi-\text{wall})-(\text{I})}$ can be obtained by looking at Figure 7. We emphasize here that the order of magnitude of velocity $v_{(\pi-\text{wall})-(\text{I})}$ remains the same over the whole $\beta-$range ($v_{\max}/v_{\min} < 3$). An important parameter that greatly affects the qualitative behaviour of the system is the characteristic time $\tau_{\text{I}}(\beta) = \ell/v_{(\pi-\text{wall})-(\text{I})}$ needed by the interface to move a macroscopic length ℓ over the NLC sample. A typical experimental value is $\tau_{\text{I}} \approx 100$ s for $\ell = 1$ mm, $\beta = 80°$ and $H = 7.7$ kG. This time is expected to be an almost-linear function of $1/H$.

5.2. INHOMOGENEOUS-HOMOGENEOUS $\pi-$WALL RELAXATION. — In this Section, we are interested in understanding why the relaxation of the $\pi-$wall texture can be either homogeneous or inhomogeneous, depending on the β and H values.

Figure 15a shows the cell 51 s after switching on a magnetic field $H = 7.7$ kG at an angle $\beta = 79°$. One can distinguish a white domain corresponding to domain A ($\pi-$wall texture) and several dark domains corresponding to domain B (texture (I)). In Figures 15b-d, we show the same region of the cell for different β, $\beta = 81°$ in Figure 15b to $\beta = 83°$ in Figure 15d and at different times after switching on the magnetic field. We see clearly that as β is increased, the domains B become more and more diffused everywhere in the NLC layer and the contrast between the different domains decreases. For $\beta = 84°$, the domains do not appear and the relaxation of the system is nearly *homogeneous* everywhere. Therefore $\beta = \beta_{\text{c}} \approx 84°$ is a nearly critical angle for the transition from the inhomogeneous dynamical regime to the homogeneous one. Moreover, to obtain the nucleation of domain B in almost all sites in the four Figures 15 we must wait a much shorter time t_H by going from Figure 15a with $t_H = 51$ s to Figure 15d with $t_H = 1$ s. This is in agreement with the exponential dependence on β of the characteristic time τ_{W} in (3.21). The critical angle β_{c} for the transition from the homogeneous relaxation to the inhomogeneous relaxation is an increasing function of the intensity H of the magnetic field. In particular, for $H \leq 2$ kG we observe the homogeneous regime for any $\beta-$value.

In the inhomogeneous regime, domain B nucleates always at the same points on the surface. Thus, the nucleation mechanism is predominantly due to surface inhomogeneities. To understand the homogeneous-inhomogeneous transition, we must compare the homogeneous relaxation time $\tau_{\text{W}}(\beta)$ with the time $\tau_{\text{I}}(\beta)$ that is needed for texture (I) to spread throughout the observation region of the sample. According to Section 5.1, $\tau_{\text{I}}(\beta)$ is a smooth function of β and, thus, can be assumed to have the same value at any point of the NLC layer. On the other hand, $\tau_{\text{W}}(\beta)$ is an exponential function of β that, for $\xi \ll d$, changes by some order of magnitude for a small change of the surface angle β. Due to the presence of small surface inhomogeneities, β ranges from a minimum value $\beta_{\min}$ to a maximum value $\beta_{\max}$ and $\tau_{\text{W}}(\beta)$ ranges from $\tau_{\text{W}_{\max}}$ to $\tau_{\text{W}_{\min}}$

Therefore there are two possible cases:

(a) $\tau_{\text{W}_{\max}} \ll \tau_{\text{I}}$. The system relaxes homogeneously;

(b) $\tau_{\text{W}_{\max}} \geq \tau_{\text{I}}$. B-domains nucleate in those regions having the highest surface angle β and spread everywhere in the NLC layer before the homogeneous transition to texture B can occur in the other regions. Thus, the critical angle $\beta_{\text{c}}(H)$ is set $\tau_{\text{W}}(\beta_{\text{c}}) \approx \tau_{\text{I}}$. This qualitative behaviour is in satisfactory agreement with the experimental observations.

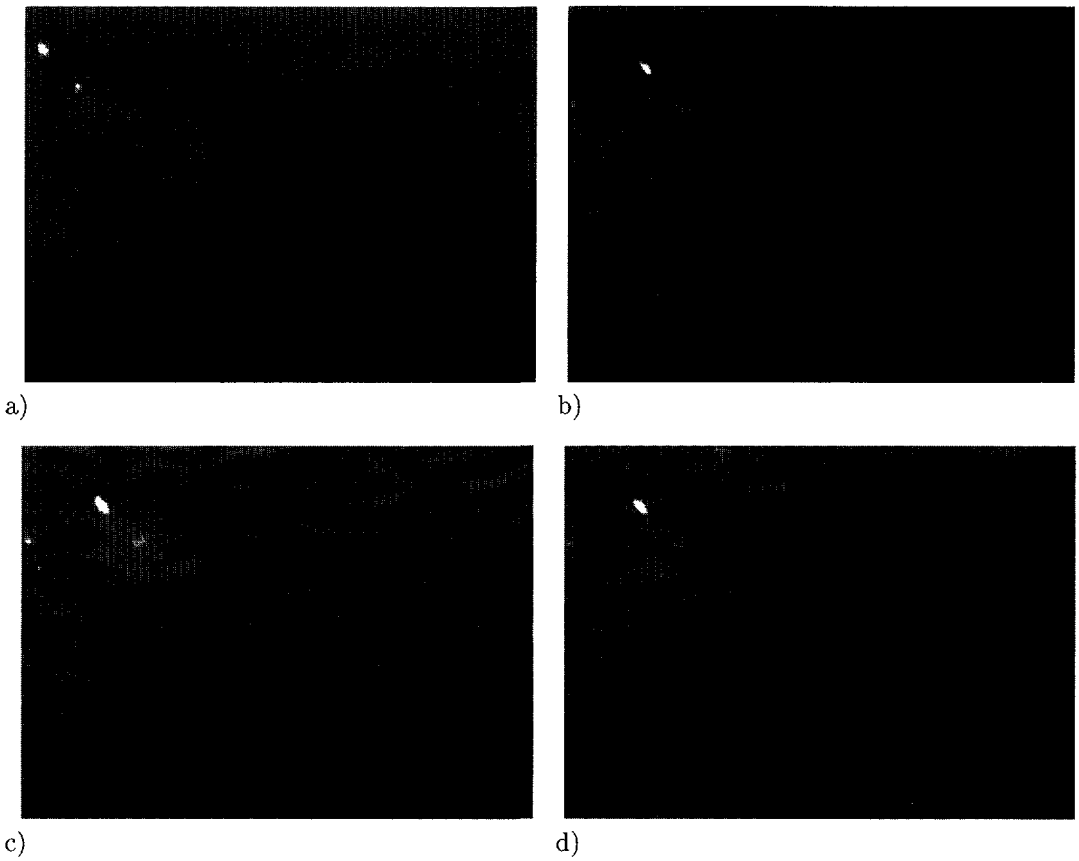

Fig. 15. — Cell in transmitted light. The polarizers are parallel ($\alpha_P = \alpha_A = 75°$). The length scale is the same as in Figure 3. The four photos correspond to the same applied magnetic field $H = 7.7$ kG, but at different angles β and time intervals t_H after the magnetic field is switched on. In particular: (a) $\beta = 79°$, $t_H = 51$ s. (b) $\beta = 81°$, $t_H = 9$ s. (c) $\beta = 82°$, $t_H = 3$ s. (d) $\beta = 83°$, $t_H = 1$ s. The dark and white regions represent domain B and domain A, respectively.

The analysis above seems to suggest a gradual crossover between the homogeneous and the inhomogeneous regime. On the contrary, the experimental data suggest a singular behaviour (bifurcation). This apparently critical behaviour is caused by the exponential dependence of τ_W on the β-angle. For sufficiently high magnetic fields ($d \gg \xi$), a small variation of the β-angle is sufficient to change τ_W by some order of magnitude. This special feature makes the crossover between the homogeneous and the inhomogeneous regime very sharp in the high-magnetic-fields region. A more gradual transition is observed at lower magnetic fields.

6. Conclusions

We have studied the inhomogeneous dynamical regime of a $+\pi/2$ twisted nematic layer under a magnetic field parallel to the layer plane. Such a special geometry leads to a very rich dynamical behaviour with the appearance of domains corresponding to unstable, metastable and stable textures with related line defects and walls. The simultaneous use of a transmitted-light and

a reflected-light experimental technique, allows us to characterize the different textures and to compare them with the theoretical predictions.

Three different textures and interfaces appear: an unstable texture of slow decay, a metastable texture and finally a wholly stable texture. The transition from the unstable and metastable textures to the stable texture occurs only inhomogeneously by nucleation of disclination lines. By contrast the unstable texture relaxation toward the metastable texture can occur either homogeneously or inhomogeneously. Two different characteristic times τ_W and τ_I control the character of this transition.

References

[1] de Gennes P.G. and Prost J., The Physics of Liquid Crystals, II ed. (Clarendon Press, Oxford, 1993).
[2] Hurd A.J., Lonberg F., S. Fradeu and Meyer R.B., *Phys. Rev. Lett.* **52** (1984) 1903.
[3] Leger L., *Solid State Commun.* **11** (1972) 1499.
[4] Faetti S., Carlotti L. and Nobili M., *submitted to Liq. Cryst.*
[5] Chandrasekhar S. and Ranganath G.S., *Adv. Phys.* **35** (1986) 507.
[6] Kleman M., *Rep. Prog. Phys.* **52** (1989) 555.
[7] Boix M., Monkade M. and Durand G.. *Europhys. Lett.* **5** (1988) 697.
[8] Palleschi V., Faetti S. and Schirone A., *Il Nuovo Cimento* **10** (1988) 1313.
[9] Nobili M., Faetti S. and Raggi I., *J. Phys. II France* **4** (1994) 287.
[10] Nobili M., Faetti S. and Schirone A., *Liq. Cryst.* **10** (1991) 95.
[11] Elsgolts L., Differential Equations and the Calculus of Variations, chapter **8** (Mir Publishers, Moscow, 1977) pp. 369–388.
[12] Oldano C., Allia P. and Trossi L., *Phys. Scr.* **37** (1988) 755.
[13] Brochard F., *J. Phys. France* **33** (1972) 607.
[14] Faber T.E., Bunning J.D. and Sherrel P.L., *J. Phys. France* **42** (1991) 1175.
[15] Cladis P.E., van Saarloos W., Finn P.L. and Kortan A.R., *Phys. Rev. Lett.* **58** (1987) 222.
[16] Ryskin G. and Kremenetsky M., *Phys. Rev. Lett.* **67** (1991) 1574.
[17] Gatti M., Faetti S. and Palleschi V., *J. Phys. Lett. France* **46** (1985) 881.
[18] Scherrel P.L. and D.A. Crellin D.A., *J. Phys. Colloq. France* **40** (1979) C3–213.
[19] J.H. Coles and M.S. Sefton. *Mol. Cryst. Liq. Cryst. Lett.* **36** (1976) 51.